Droplet on a sugar fiber

Stéphane Dorbolo [*]
F.R.S.-FNRS, UR-CESAM, PtYX laboratory, Université de Liège, Liège, Belgium

Floriane Weyer
Haute Ecole Charlemagne, Liège, Belgium

Alexandre Delory
ENS Lyon, CNRS, LPENSL, UMR5672, 69342, Lyon cedex 07, France

Apurav Tambe and Zhao Pan
Mechanical and Mechatronics Engineering, University of Waterloo, Canada

(Received 8 July 2025; accepted 10 February 2026; published 9 March 2026)

The motion of a water droplet on a single vertical sugar fiber is analyzed. The fiber is positioned vertically, with the droplet placed at its pending end. If the capillary force is able to balance the weight of the droplet, the droplet remains suspended at the fiber extremity. As sugar is dissolved inside the droplet, the fiber eventually breaks. Subsequently, the droplet may fall down carrying a portion of the not yet dissolved fiber, or, more interestingly, the droplet may be propelled upwards, remaining attached to the fiber. The process can then restart. The upward jump (or motion) of the droplet is caused by the capillary force exerted by the droplet on the fiber. When the fiber breaks (or becomes weakened) due to dissolution, this capillary force is no longer balanced, causing the droplet to jump upward. A phase diagram is constructed based on the droplet volume and the fiber diameter. A model has been built to assess the critical droplet volume for a given fiber diameter, above which the droplet falls. Below this volume, the droplet can move upwards along the fiber.

DOI: 10.1103/p39v-8wss

I. INTRODUCTION

Droplet interaction with fiber(s) is common in nature and in daily life. That can be as simple as a rain droplet hitting the fabric of a coat or a spider web. The equilibrium position and motion of a droplet along a fiber are even more complex than wetting on a planar surface. Indeed, the fiber's curvature must be considered, together with the direction of gravity or any other external forcing. As a result, droplet size becomes important: its volume governs both its shape and its behavior along the fiber. Besides the fundamental challenges, the droplet-fiber interaction is relevant in numerous applications. The glass wool production process implies to use binder droplets to ensure a good adhesion between the glass fibers [1]. Passive fibers are used in filtering processes [2], cooling process [3], or dew harvesting [4]. In other situations, they offer a unique configuration for studying fluid dynamics, for example, when an immersed fiber is employed to observe the dilution of a liquid droplet in another liquid [5,6]. The natural fibers found in the biosphere also inspired scientists. Spider silk, for instance, relies on capillary forces: fine sections of silk fiber are embedded in hanging liquid droplets, creating a composite system providing the fiber elasticity [7]—a principle

[*]Contact author: s.dorbolo@uliege.be

that has since been adapted for dew harvesting [8]. Fiber geometry also plays a significant role in droplet behavior. The conical shape of cactus spines allows guiding water droplets toward the base, a strategy that has led many experimental and numerical explorations of other geometrical configurations and orientations [9–14]. Additionally, it has been shown that when fibers come into contact, transport properties are enhanced [15], and even more when the fibers are twisted [16].

When the fiber is horizontal, the shape adopted by the droplet around the fiber has been demonstrated to depend on the nature of the liquid and the fiber. Yet, the volume of the liquid involved is still relevant. Moreover, besides the nature of the fiber material, its surface roughness may drastically change the droplet shape and behavior along the fiber. According to the gravity orientation with respect to the wire, to the volume of the droplet, to the contact angle and to the diameter of the fiber, the droplet may adopt either a symmetrical shape named "barrel" or an asymmetrical shape, named "clamshell" [17–19].

The motion of the droplet on the fiber can be triggered by inclining the fiber. For a given droplet volume that depends again on the nature of the liquid and the fiber, the droplet starts moving downwards [20–22]. The apparent droplet contact angles at the front and rear correspond to the advancing and receding values, respectively. Numerical simulations were performed to describe a droplet on a vertical fiber [23].

Besides the orientation of the gravity, the environment of the fiber matters. When exposed to a lateral wind, the droplets may move [24,25]. In a similar manner, vibration introduced by sound can be used to expel the droplet from the fiber [2,26]. The opposite situation, namely the impact of a droplet on a fiber, was also investigated since this problem is relevant for the capture of liquid by a network of fibers [27–29].

Finally, the deformation of the fiber stands for an interesting degree of freedom regarding applications in textile, for example. The fiber can be flexible [30], and the presence of the liquid may change the properties of the fiber by swelling [31]. In an analog manner, a water droplet that sits on a sugar fiber locally changes the physical properties of the fiber. Indeed, the liquid dissolves the fiber modifying the local radius of the fiber and its elasticity as the water invades the sugar structure. In this paper, we propose to study the fate of a vertical sugar fiber on the extremity of which, a droplet of water was released. Lumberjacks know that sawing the branch on which you sit results in a fatal issue. Droplets experience a different story.

II. EXPERIMENTAL SET UP

The method for producing the sugar fiber is similar to the experimental procedure found in Ref. [32]. The aim was to obtain a regular and cylindrical fiber. The sugar fibers were made from glucose (Alpha-Sigma, Aldrich Chemical Company, USA). Some grams of glucose were heated on a temperature-controlled hot plate. The temperature was fixed to 110 °C. At that temperature, the glucose melts without caramelizing [Fig. 1(a)]. While the sugar was liquid, a drop was captured using a wooden stick. The droplet was then transferred to a room-temperature plastic substrate to be gently squeezed between the stick and the support. The stick was then pulled up at a constant speed v_{up} (about 1 cm/s), extending the fiber between the plastic plate and the stick tip. Sometimes, air bubbles were trapped during the process, and we discarded the flawed fibers.

The fiber was vertically attached to a horizontal plate (Fig. 1). Fibers were not misaligned for more than a few degrees regarding the vertical direction. A water droplet was then released at the free end of the fiber in such a way that it did not wet the remaining length of the fiber. A backlight allowed obtaining highly contrasted images that were captured by a camera (JAI BM-500, Edmund Optics, USA). Three pictures were taken for each considered case (i.e., a combination of the droplet volume V and fiber diameter d): the naked fiber, the fiber loaded with the droplet, and the outcome after the fiber dissolution.

The image analysis result is shown for one case in Figs. 1(b)–1(e). An in-house Python script (built with OpenCV) was used to measure the fiber diameter and estimate the volume of the droplet-covered section of the fiber [Figs. 1(b) and 1(c)]. The code also allows to extract and estimate the

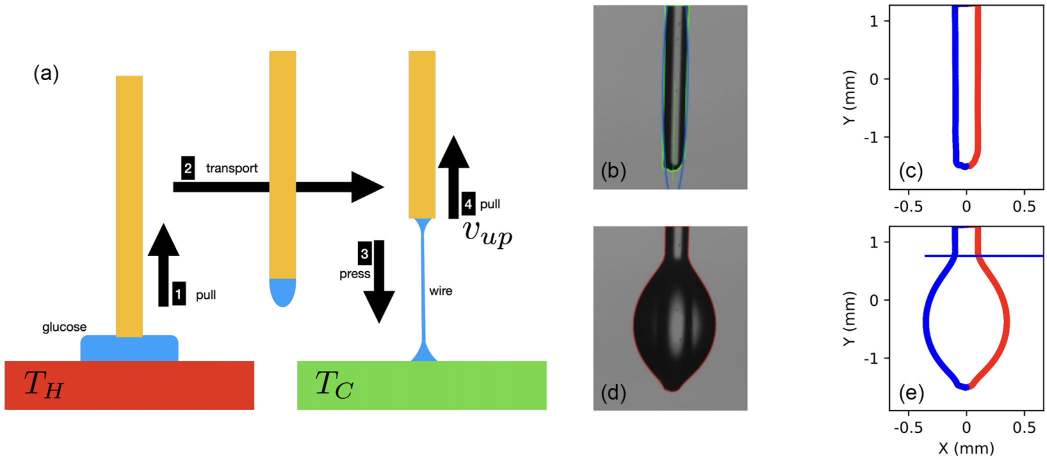

FIG. 1. (a) Schematic procedure to obtain a sugar fiber. The solid glucose was heated at $T_H = 110\,^{\circ}\mathrm{C}$ to melt. A rod was plunged in the liquid sugar and was pulled out of the puddle. A droplet of sugar was transport towards a cold plate (T_C is room temperature). The droplet was squeezed in between the rod and the cold plate. The rod was pulled up with a constant speed $v_{\rm up}$ generating a fiber of sugar. (b)–(e) Image analysis of a droplet pending at the extremity of a sugar fiber. (b), (d) Images of the fiber without and with a droplet respectively, and (c), (e) the corresponding plots after image analysis. The contour of the fiber is in green (b) and the contour of the droplet in red (d). The blue ellipse (b) is a fitted ellipse that allows to obtain the main axis of the fiber. Red and blue colors in (c), (e) correspond to right and left profiles of the images. The horizontal line in (e) corresponds to the determination of the contact line. In the present case, we measured the droplet vertical extension $L = 2.33$ mm, the volume $V = 1.73$ mm^3, and the fiber thickness $d = 387$ µm.

volume of the droplet, taking into account the volume of the fiber inside the droplet [Figs. 1(d) and 1(e)].

The image of a fiber without a droplet attached [Fig. 1(b)] was first analyzed to get the shape of the fiber [Fig. 1(c)]. Both sides of the fiber were measured separately, in red and blue. Then, the image with the droplet [Fig. 1(d)] allowed to extract the droplet profile [Fig. 1(e)]. The droplet surface S and volume V were estimated by invoking the rotational invariance of the profiles around the fiber's axis of symmetry. Measurements for both sides were then averaged, and the droplet volume V was ultimately obtained after the subtraction of the fiber volume.

III. RESULTS

The geometrical configuration of the droplet sitting at the extremity of the fiber remains unchanged during the dissolution process of the fiber which takes around minutes (according to the diameter of the fiber). This explains why three pictures are necessary and sufficient to define the dissolution dynamics from the geometrical point of view. However, some fluid motion can be observed inside the droplet during the dissolution process. The flow was evidenced because of the presence of dusts or because of the local density contrast due to the presence of sugar. Some movies are presented in the Supplemental Material [33]. The observed motion of the fluid is a flow that goes downwards along the fiber and upwards along the surface of the droplet. Close to the fiber, the water is rich in sugar; the local density being larger than the rest of the droplet, the liquid locally sinks. In total, a gradient of sugar concentration builds up between the bottom and the top of the droplet. The main consequence is that the dissolution of the fiber by the droplet is not homogeneous: the fiber dissolves faster at the top of the droplet since the local concentration of sugar is lower than at the bottom. Since the fiber thins, it may eventually break. Two possible outcomes are thus reported: either the droplet detaches and falls due to gravity, or it is propelled upward and remains adhered to the fiber.

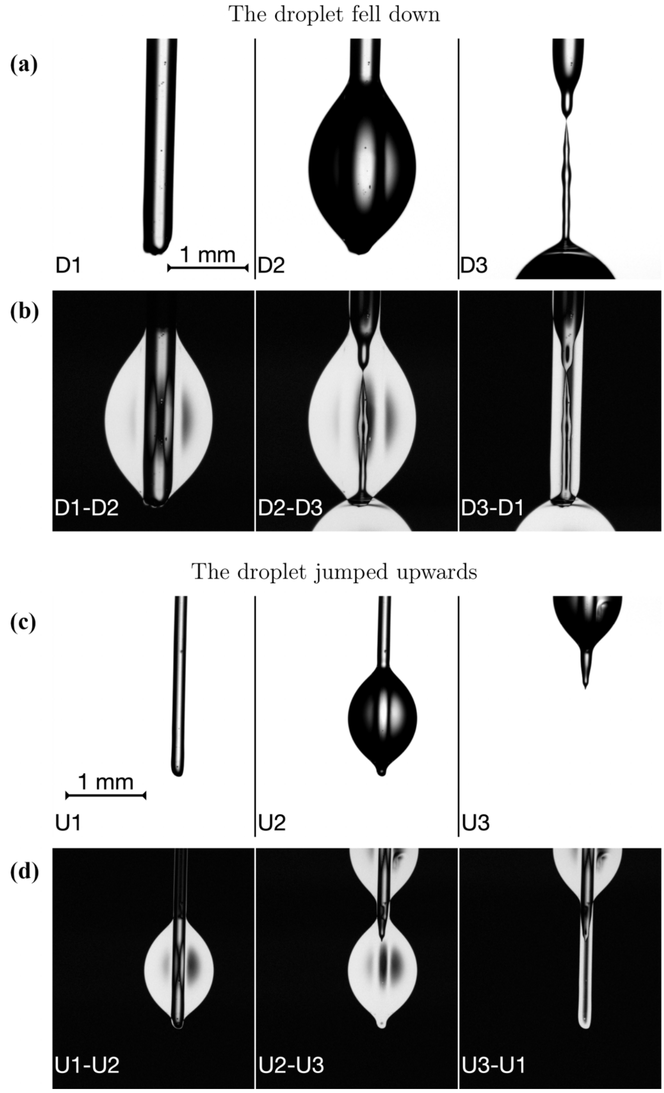

FIG. 2. Presentation of the two possible outcomes after the dissolution of the fiber: either (a), (b) the droplet falls down (denoted by the letter "D") or (c), (d) goes upwards (denoted by the letter "U"). Rows (a), (c): Pictures of the fiber alone (D1, U1), of the fiber and the droplet just after the release of the droplet (D2, U2), and of the outcome just after the motion of the droplet (D3, U3). In the case "D", the fiber diameter was $d = 387\,\mu$m, the droplet vertical extension L and volume V were 2.33 mm and 1.73 mm^3. In the case "U", $d = 163\,\mu$m, $L = 1.41$ mm, and $V = 0.450$ mm^3. The dark images in (b), (d), result from the subtraction of two images as explicitly written, e.g., U1 − U2 means the subtraction of image U1 and image U2. D1 − D2 and U1 − U2 evidence the contact angle and the position of the droplet on the fiber. D2 − D3 and U2 − U3 indicate where the water has most significantly altered the fiber. Finally, D3 − D1 and U3 − U1 allow for comparing the initial and final shape of the fiber.

Two examples of analyzed images are reported in Fig. 2. Both scenarios are presented. The first two rows (a), (b) correspond to a case for which the droplet fell down after the sugar fiber had been dissolved, and corresponding images are denoted with the letter "D". The diameter of the fiber was $d = 387\,\mu$m and the volume of the droplet $V = 1.73$ mm^3. The two rows at the bottom (c),

(d) correspond to a case of a droplet that jumped upwards and are denoted with the letter "U". The fiber diameter was $d = 163$ µm and the volume of the droplet $V = 0.450$ mm^3. Note that we chose a case "D" for which the fiber did not break completely in order to better illustrate how the fiber shape evolves during the dissolution process. Indeed, we can see the presence of a thin region just below the initial position of the top contact line.

In Figs. 2(a) and 2(c) (white background), we can see the naked fiber on the left-hand side (D1 and U1) and the pending droplet just after its release on the extremity of the fiber in the middle (D2 and U2). In the last row (D3 and U3), we can see the position of the droplet just after its motion at the end of the process, i.e., pending at the extremity of the fiber (D3) and at the upper part of the fiber (U3).

To better evidence the dissolution dynamics, pictures of Fig. 2 have been subtracted from each other. More precisely, images "D1-D2" and "U1-U2" allow a direct visualization of the contact angles of the droplet with the fiber. In both cases, one can see that the droplet shape at the bottom resembles the classical Young-Dupré configuration. The contact line is pinned along the perimeter of the fiber extremity. On the contrary, the droplet shape close to the top contact angle exhibits a change of curvature. The contact angle at the top contact line is small (we estimate $<5°$). Images $\mathrm{D2} - \mathrm{D3}$ and $\mathrm{U2} - \mathrm{U3}$ reveal the position of the upper contact line on the fiber and its location relative to the thinnest section of the fiber. In both cases, the contact line of the top is located well above (more than one fiber diameter length) the weakest part of the fiber. Finally, $\mathrm{D3} - \mathrm{D1}$ and $\mathrm{U3} - \mathrm{U1}$ show the global change of shape of the fiber due to the dissolution process.

In total, 93 cases were studied for droplet volume V ranging from 0.032 to 3.5 mm^3 and for fiber diameter d ranging from 125 to 542 µm. Among these 93 cases, 48 droplets jumped upwards.

A. Contact angle

The average contact angles θ at the bottom were manually measured from the images (i.e., $\mathrm{D1} - \mathrm{D2}$ and $\mathrm{U1} - \mathrm{U2}$) by taking the averaged values of the angles at the left and right hand side of the apparent contact line. The apparent contact angle at the bottom, which is an advancing contact angle, was found to range from 20 to 60°. On the other hand, if one zooms in near the top contact line, the apparent contact angle is harder to define because of the continuous change of curvature of the droplet profile at the receding contact line. Yet, we can argue that the apparent receding contact angle is smaller than 5°. Indeed, the liquid seems to perfectly wet the sugar since the water is dissolving it. The observed difference between the top and bottom angles is due to gravity pulling the droplet downwards, as well as the presence of the edge at the bottom fiber extremity that pins the contact line.

In a first-order approach, we consider that the capillary force acting on the droplet is similar to the case of a droplet on an inclined fiber or plane. Following Furmidge's idea [34] (see also recent work by McHale [35]), this force writes

$$F_c = \pi d \gamma [\cos(\theta_r) - \cos(\theta_a)],$$

where θ_r and θ_a are the receding and advanced contact angles, respectively, and γ is the surface tension. The calculated bottom contact angle θ_c, that we identify to θ_a, can be found by balancing F_c and the droplet weight

$$\cos(\theta_c) = \cos(\theta_r) - \frac{\rho V g}{\pi d \gamma}, \tag{1}$$

where ρ is the density of water (at first approximation).

Two scenarios are envisaged. The first one considers that the receding contact angle is equal to zero as an asymptotic case, $\theta_r = 0$. Within this hypothesis, the averaged measured angle θ at the bottom of the droplet (i.e., the average of the measured apparent contact angle at the right and left) is plotted as a function of the calculated one, $\theta_c(\theta_r = 0)$, in Fig. 3(a) (red discs). A good correlation is found since the solid line is a fit by $a + \theta_c$ where a is a fitting parameter found here to be equal

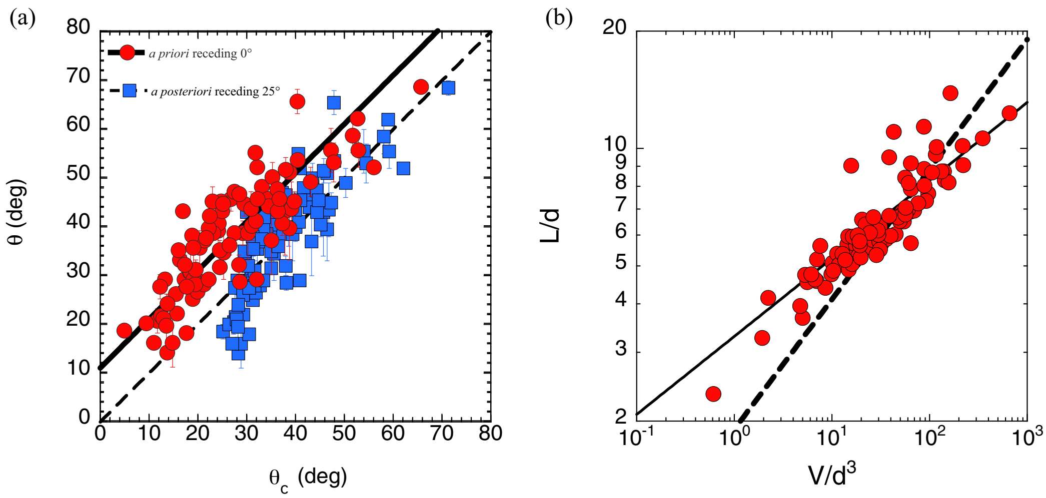

FIG. 3. (a) Bottom contact angle θ (see text) as a function of the calculated contact angle following Eq. (1) for a receding contact angle fixed at zero (red discs) and for an optimized receding contact angle (blue squares). The line is a linear fit with a slope equal to unity to the red discs, while the dashed line corresponds to the main bisector. (b) Log-log plot of the normalized length L/d of the droplet when sticking to the fiber as a function of the normalized droplet volume. The dashed and the solid curves correspond to a power law $L/d \propto (V/d^3)^{1/3}$ and to $L/d \propto (V/d^3)^{1/5}$.

to $10^\circ \pm 0.6^\circ$. Actually, regarding the main bisector represented by the dashed line in Fig. 3(a), the dispersion is rather large. However, the parameter a indicates that the law in Eq. (1) underestimates the advancing contact angle. This may be due to the pinning of the droplet at the angular extremity of the fiber. Indeed, we wanted as much as possible to work on dry fiber instead of wet fiber (see Sec. III E). Thus, we released the droplet directly close to the extremity. If the droplets were released at any other place on the fiber, most of the droplets would have slid along the fiber. In the considered cases, the edge blocked any motion of the droplet by pinning the contact line. Consequently, the angle measured at the bottom of the droplet could be larger than the calculated advancing angle.

The second method involves treating the receding contact angle as a free parameter and optimizing its value to best match the main bisector (θ_c, θ) (least squares method). The optimized $\theta_{r,\mathrm{opt}}$ was found to be equal to 25°. The measured value of the droplet contact angle at the fiber extremity θ is reported as a function of the calculated angle using the optimized contact angle, i.e., $\theta_c(\theta_r = \theta_{r,\mathrm{opt}})$ in Fig. 3(a) (blue squares). However, we have to note that the value of the optimized contact angle is much larger than the observed one.

On the whole, the Furmidge formula is a fair approximation of the force acting on the droplet. However, some adaptations should be considered. First, the droplet is not moving, and the contact angle at the bottom contact line has to accommodate the edge of the fiber. Second, the droplet seems to completely wet the fiber because of the dissolution of the sugar, yielding a very small contact angle at the upper contact line. Third, the surface tension and the density of the liquid vary in time and space because of the dissolution and the sugar concentration gradient in the droplet.

B. Fiber shape and droplet shape

From "D3-D1" and "U3-U1", we can visualize the fiber shape inside the droplet just before the motion of the droplet. One can see the inhomogeneous dissolution of the fiber. It becomes conical close to the contact line between the droplet and the fiber. The fiber is not the thinnest at the top contact line, but just below. This is particularly obvious and spectacular on "D3", where the thinnest fiber dimension is of about three pixels (smaller than 5 μm) without breaking.

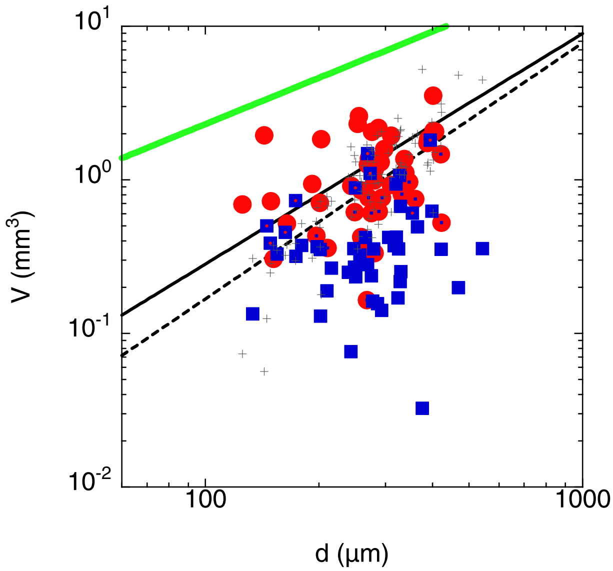

FIG. 4. Phase diagram (log-log scale) for the climbing (blue squares) and falling droplets (red discs) as a function of their volume V and of the fiber diameter d. Below the green line [Eq. (2)], the droplet can remain on the fiber. Gray crosses $V^{\star}(d)$ indicate the threshold volume below which the droplet is supposed to go upwards for each V-d couple; they are calculated using Eq. (5). When the data point does not follow the model, an additional inner symbol is added to the main symbol. The dashed line is the power law $V^{\star} \propto d^{5/3}$ from Eq. (6), while the black line is the power law $V^{\star} \propto d^{3/2}$ from Eq. (7).

When the droplet sits at the extremity of the fiber, regarding the geometry, three parameters can be measured (see Sec. II): the droplet volume V, its vertical extension L along the fiber, and the fiber diameter d. For a given volume V, the droplet spreads a distance L along the fiber and makes a contact angle θ at the fiber extremity. The normalized vertical extension L/d is reported as a function of the normalized volume $V_d = V/d^3$ in Fig. 3(b). In Refs. [22,23], the vertical extension of the droplet is found to scale as $L/d \approx 1.24\, V_d^{1/3}$. In Fig. 3(b), the dashed line corresponds to a fit $L/d = A\, V_d^{1/3}$. In so doing, we find $A = 1.90$, which is about 50% above the predicted value. This is probably due to the affinity of the water with the sugar (the droplet spreads along the fiber) or to the deposition process. On top of it, we propose to fit the data using a phenomenological law, the solid curve corresponding to a fit $L/d = B\, V_d^{1/5}$ with $B = 3.3$. For both, the greater the volume, the further the droplet spreads.

C. Phase diagram

The 93 droplets of various volumes V sitting on fibers of various diameters d have been considered to build up a phase diagram, jumped or fell. For each V-d couple, the outcome of the dissolution was recorded, namely if the droplet fell down or jumped upwards on the fiber. The results are plotted in a log-log plot in Fig. 4 where the data point is a blue square when the droplet jumped and a red disk when the droplet fell down. Blue squares and red discs are rather mixed for volumes below 0.7 mm^3. On the other hand, the discs are mainly located above this limit. This suggests that a criterion exists to predict whether the droplet would fall down. In theory, this also corresponds to the criterion that determines whether the droplet should jump upwards. But, in practice, failure remains possible: a droplet predicted to jump may instead be observed to fall. Note that the reverse situation cannot occur, i.e., a droplet predicted to fall down is unlikely to jump.

D. Model

To start with, we can evaluate the criterion for the volume above which the droplet simply slides and falls. Since the droplet is attached to the fiber, a simple condition for the attachment is that the maximum weight $W^\star$ of the droplet equals the maximum capillary force $F_c = \pi d\gamma$. This condition simply reads

$$W < \pi d\gamma, \tag{2}$$

where γ is the surface tension of the water (72 mN/m). The force is said to be maximum because Eq. (2) already assumes that the droplet totally wets the fiber, which is roughly the case since we observed a small contact angle at the upper contact line.

As the weight is given by $\rho V g$, where ρ is the density of water, we can deduce the maximum volume $V_{\max}$ that a fiber of diameter d can hold

$$V_{\max} = \frac{\pi d\gamma}{\rho g}.$$

This theoretical upper bound is reported as the green curve in Fig. 4. All the data points are, of course, located below this limit since the reported data concerned only cases when the droplet falls after having dissolved the fiber.

We observed that the condition for dropping or jumping upwards is related to the droplet volume and the fiber diameter. When the droplet stands on the fiber during the dissolution process, capillary forces apply at the top and at the bottom contact line. The wetting process tends to spread the droplet along the fiber, which is possible in the upward direction, but not at the bottom since the contact line is pinned at the fiber extremity. On the whole, the piece of fiber located inside the droplet is longitudinally compressed. When the fiber breaks, the bottom capillary force $F = \gamma\pi d\cos(\theta)$, with θ the contact angle at the bottom of the droplet, is not balanced anymore by the compression in the fiber. This force induces a vertical acceleration of the droplet during a typical time given by the capillary time $\tau_c = \sqrt{m/\gamma}$, with $m = \rho V$ the droplet mass. The maximum vertical speed v_{jump} can be evaluated after a time $t = \tau_c$:

$$v_{\text{jump}} = \frac{F}{m}\tau_c = \pi d\cos\theta\sqrt{\frac{\gamma}{\rho V}}. \tag{3}$$

To remain attached, the droplet must jump a height at least equal to its vertical extension L. Since the fiber is broken, the droplet is affected by gravity. The minimal speed $v_{\min}$ to move vertically of a distance L is thus evaluated by

$$v_{\min} = \sqrt{2gL}. \tag{4}$$

A basic criterion to remain attached is obtained by comparing v_{jump} and $v_{\min}$. This equality allows defining the critical volume $V^\star$ below which the droplet may jump upwards and remain attached to the fiber, namely,

$$V^\star(d) = \frac{\pi^2 d^2\gamma\cos^2\theta}{2\rho g L}. \tag{5}$$

Taking the measured θ and the measured L, we can compute the threshold $V_c(d,\theta,L)$ for each considered V-d couple. They are reported in Fig. (4) by gray crosses. Consequently, we can evaluate whether the droplet was supposed to jump upwards or to fall according to our model. If the data point is above the corresponding cross, the droplet was predicted to fall, but if the data point is below, the droplet was predicted to jump upwards. In case of a mismatch between the prediction and the observation, the symbol was surcharged with the symbol of the prediction, namely a blue square if the droplet was supposed to go up and a red circle if the droplet was supposed to fall down. The model makes two types of errors. It incorrectly predicts falling in 6 out of 48 cases where the droplet actually jumped upward, and it predicts upward jumps in 20 out of 45 cases where the

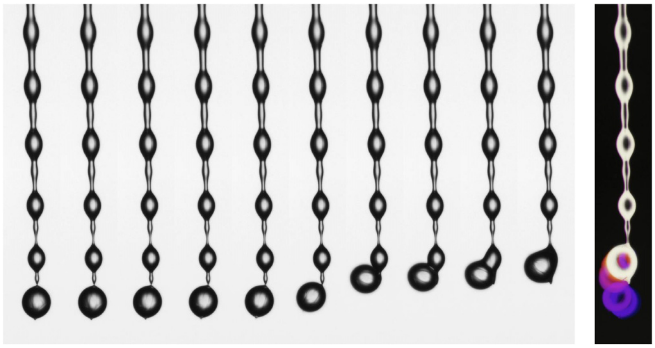

FIG. 5. Successive snapshots of a prewet sugar fiber. The time delay between two images is 85 ms. On the right, the image is obtained by summing the successive snapshots.

droplet actually fell. Indeed, the failure of the upward motion is due to uncontrolled parameters such as the fiber anisotropy, vibrations, and the initial position of the droplet. On the whole, we can conclude that the criterion can predict the fate of the droplet knowing the droplet volume, the contact angle, and the vertical extension L.

A model that predicts the droplet vertical extension is still to be adapted to the case of a soluble fiber. First, we can try to extract an empirical law for the criterion Eq. (5) by introducing the phenomenological law for the extension $L = B'V^{1/5}$, where $B' = 0.12$ m$^{2/5}$. If we neglect the variation of the contact angle with the volume by taking a fixed average angle $\bar{\theta} = 38.15°$, we have that

$$V^\star = 7.8 \times 10^{-5} d^{5/3}. \tag{6}$$

Second, the same exercise is performed considering the scaling for L proposed by Ref. [22] and discussed earlier, i.e., $L = AV^{1/3}$. In so doing, we find

$$V^\star = 2.8 \times 10^{-4} d^{3/2}. \tag{7}$$

We plotted Eqs. (6) and (7) as a dashed and a continuous black line in Fig. 4. Since these criteria are partially based on Eq. (5), it is not surprising that both models separate the blue squares and red discs well. In addition, the mixed symbols (red dots in blue squares or blue squares in red discs) are all located around the phenomenological curve. We may treat them as transit cases due to numerous influences like inhomogeneities in the fiber, vibrations, etc. These observations further validate Eq. (5) as a good model. Yet, the scaling models in Eqs. (6) and (7) allowed to provide a rapid criterion for the droplet fate after the dissolution of the fiber.

E. Wet sugar fiber

The situation is rather different when the sugar fiber is beforehand wet by the passage of the droplet. To illustrate this, a large droplet was released close to the top attachment point of the fiber. The droplets slid down and wet the fiber before detaching when they reached the lower extremity of the fiber. After the passage of the large droplet, a film of water was released along the fiber. Dissolution begins, and the remaining liquid film, made up of water and sugar, reveals a Rayleigh-Plateau instability. In Fig. 5, the time lapse of such a wet fiber is shown. The time delay between two successive images is 85 ms. Since the deposition of liquid is rather minimal, one expects to observe the jump of the droplet located at the fiber bottom extremity. Sometimes, the droplets may fall down or jump, and sometimes the fiber may collapse. However, we observed several times another interesting behavior: the fiber bends inside the droplet since the surface tension compresses the fiber inside it. This bending may result in a rotation of the fiber and a global upwards motion of the droplet (see [33]). Note here that prewetting is not necessary; if the air moisture is sufficient, then water may adsorb on the fiber before dissolving it, following the same scenario.

IV. CONCLUSION

A droplet of water pending at the extremity of a vertical sugar fiber has a contact line located along the bottom fiber edge and another one located on the fiber. Surface tension compresses the fiber located inside the droplet, and water dissolves the fiber made of sugar. The dissolution is not homogeneous due to the induced sugar concentration gradient in the droplet under the action of gravity. As a consequence, the fiber gets thinner faster close to the upper contact line until the fiber eventually breaks.

A criterion that accounts for the fiber diameter, the contact angle, the vertical extension, and the volume of the droplet has been defined and allows to predict wether the droplet falls or jumps. If this criterion is satisfied, the droplet may remain attached to the fiber, and the dissolution process may restart. Eventually, the droplet liquid reaches a high sugar concentration, resulting in a density increase and in the falling of the droplet. Other mechanisms, such as droplet rotation or fiber bending, were observed with prewet fibers after the development of a Rayleigh-Plateau instability.

ACKNOWLEDGMENTS

S.D. is a F.R.S.-FNRS Senior Research Associate. Part of this work was financed by UR-CESAM. A.T. and Z.P. are thankful for support from the Natural Sciences and Engineering Research Council of Canada (NSERC), Discovery Grant, RGPIN-2020-04486 and National Research Council Canada (NRC), A14D-147.

DATA AVAILABILITY

The data that support the findings of this article are openly available [36].

---

[1] P.-B. Bintein, Dynamiques de gouttes funambules : Applications à la fabrication de laine de verre, Ph.D thesis, ESPCI-UPMC, 2015.

[2] C. Chang, Z. Wang, and Z. Ji, Experimental study on the removal of submicron droplets by fibrous filter media in a sound field, Powder Technol. **429**, 118902 (2023).

[3] Z. Yang and J. Zhang, Bioinspired radiative cooling structure with randomly stacked fibers for efficient all-day passive cooling, ACS Appl. Mater. Interfaces **13**, 43387 (2021).

[4] P.-B. Bintein, A. Cornu, F. Weyer, N. De Coster, N. Vandewalle, and D. Terwagne, Kirigami fog nets: How strips improve water collection, npj Clean Water **6**, 54 (2023).

[5] B. J. Carroll, The kinetics of solubilization of nonpolar oils by nonionic surfactant solutions, J. Colloid Interface Sci. **79**, 126 (1981).

[6] B. J. Carroll, Equilibrium conformations of liquid drops on thin cylinders under forces of capillarity. A theory for the roll-up process, Langmuir **2**, 248 (1986).

[7] H. Elettro, S. Neukirch, F. Vollrath, and A. Antkowiak, In-drop capillary spooling of spider capture thread inspires hybrid fibers with mixed solid–liquid mechanical properties, Proc. Natl. Acad. Sci. USA **113**, 6143 (2016).

[8] Y. Jiang, H. Venkatesan, S. Shi, C. Wang, M. Cui, Q. Zhang, L. Tan, and J. Hu, Spider-capture-silk mimicking fibers with high-performance fog collection derived from superhydrophilicity and volume-swelling of gelatin knots, Collagen and Leather **5**, 4 (2023).

[9] Élise Lorenceau and D. Quéré, Drops on a conical wire, J. Fluid Mech. **510**, 29 (2004).

[10] J. Van Hulle, F. Weyer, S. Dorbolo, and N. Vandewalle, Capillary transport from barrel to clamshell droplets on conical fibers, Phys. Rev. Fluids **6**, 024501 (2021).

[11] C. Fournier, C. L. Lee, R. D. Schulman, Élie Raphaël, and K. Dalnoki-Veress, Droplet migration on conical fibers, Eur. Phys. J. E **44**, 12 (2021).
[12] C. L. Lee, T. S. Chan, A. Carlson, and K. Dalnoki-Veress, Multiple droplets on a conical fiber: Formation, motion, and droplet mergers, Soft Matter **18**, 1364 (2022).
[13] Z. Pan, W. G. Pitt, Y. Zhang, N. Wu, Y. Tao, and T. T. Truscott, The upside-down water collection system of syntrichia caninervis, Nature Plants **2**, 16076 (2016).
[14] J. Zhang, H. Shen, H. Cui, L. Chen, and L. Chen, The dynamic behavior of a self-propelled droplet on a conical fiber: A lattice boltzmann study, Phys. Fluids **35**, 082119 (2023).
[15] M. Leonard, J. Van Hulle, F. Weyer, D. Terwagne, and N. Vandewalle, Droplets sliding on single and multiple vertical fibers, Phys. Rev. Fluids **8**, 103601 (2023).
[16] J. Van Hulle, C. Delforge, M. Leonard, E. Follet, and N. Vandewalle, Droplet helical motion on twisted fibers, Langmuir **40**, 25413 (2024).
[17] G. McHale and M.I Newton, Global geometry and the equilibrium shapes of liquid drops on fibers, Colloids Surf. A **206**, 79 (2002).
[18] B. J. Mullins, R. D. Braddock, I. E. Agranovski, and R. A. Cropp, Observation and modeling of barrel droplets on vertical fibres subjected to gravitational and drag forces, J. Colloid Interface Sci. **300**, 704 (2006).
[19] H. Eral, J. d. R. de Ruiter, R. de Ruiter, J. Min Oh, C. Semprebon, M. Brinkmann, and F. Mugele, Drops on functional fibers: From barrels to clamshells and back, Soft Matter **7**, 5138 (2011).
[20] B. J. Mullins, I. E. Agranovski, R. D. Braddock, and C. M. Ho, Effect of fiber orientation on fiber wetting processes, J. Colloid Interface Sci. **269**, 449 (2004).
[21] Z. Huang, X. Liao, Y. Kang, G. Yin, and Y. Yao, Equilibrium of drops on inclined fibers, J. Colloid Interface Sci. **330**, 399 (2009).
[22] T. Gilet, D. Terwagne, and N. Vandewalle, Droplets sliding on fibres, Eur. Phys. J. E **31**, 253 (2010).
[23] F. Bodziony, M. Wörner, and H. Marschall, The stressful way of droplets along single-fiber strands: A computational analysis, Phys. Fluids **35**, 012110 (2023).
[24] P.-B. Bintein, H. Bense, C. Clanet, and D. Quéré, Self-propelling droplets on fibres subject to a crosswind, Nat. Phys. **15**, 1027 (2019).
[25] J. L. Wilson, A. A. Pahlavan, M. A. Erinin, C. Duprat, L. Deike, and H. A. Stone, Aerodynamic interactions of drops on parallel fibres, Nat. Phys. **19**, 1667 (2023).
[26] S. Poulain and A. Carlson, Sliding, vibrating and swinging droplets on an oscillating fibre, J. Fluid Mech. **967**, A24 (2023).
[27] K. Piroird, C. Clanet, Élise Lorenceau, and D. Quéré, Drops impacting inclined fibers, J. Colloid Interface Sci. **334**, 70 (2009).
[28] É. Lorenceau, C. Clanet, and D. Quéré, Capturing drops with a thin fiber, J. Colloid Interface Sci. **279**, 192 (2004).
[29] E. Lorenceau, C. Clanet, D. Quéré, and M. Vignes-Adler, Off-centre impact on a horizontal fibre, Eur. Phys. J.: Spec. Top. **166**, 3 (2009).
[30] C. Duprat, S. Protière, A. Y. Beebe, and H. A. Stone, Wetting of flexible fibre arrays, Nature (London) **482**, 510 (2012).
[31] P. Van de Velde, J. Dervaux, S. Protière, and C. Duprat, Spontaneous localized fluid release on swelling fibres, Soft Matter **18**, 4565 (2022).
[32] I. Martincek, D. Pudis, and M. Chalupova, Technology for the preparation of PDMS optical fibers and some fiber structures, IEEE Photon. Technol. Lett. **26**, 1446 (2014).
[33] See Supplemental Material at http://link.aps.org/supplemental/10.1103/p39v-8wss for movies of jumping droplet.
[34] C. G. L. Furmidge, Studies at phase interfaces i. the sliding of liquid drops on solid surfaces and a therory for spray retention, J. Colloid Sci. **17**, 309 (1962).
[35] G. McHale, S. Janahi, H. Barrio-Zhang, Y. Wang, J. Chen, G. G. Wells, and R. Ledesma-Aguilar, Adhesive forces in droplet kinetic friction on liquidlike surfaces, Phys. Rev. Lett. **135**, 204003 (2025).
[36] https://doi.org/10.58119/ULG/IQWXA5.